How to improve the sensitivity of coplanar electrodes and micro channel design in electrical impedance flow cytometry: a study

Jonathan Cottet, Alexandre Kehren, Harald van Lintel, François Buret, Marie Frénéa-Robin, Philippe Renaud

How to improve the sensitivity of coplanar electrodes and micro channel design in Electrical Impedance Flow Cytometry: a study

Jonathan Cottet[1,2]. Alexandre Kehren[2], Harald van Lintel[2], François Buret[1], Marie Frénéa-Robin[1] and Philippe Renaud[2]

a Univ Lyon, Ecole Centrale de Lyon, Université Claude Bernard Lyon 1, INSA Lyon, CNRS, Ampère, F-69130, Ecully, France

b École Polytechnique Fédérale de Lausanne, EPFL-STI-IMT-LMIS4, Station 17, CH-1015 Lausanne, Switzerland

This paper describes a comprehensive analysis of the geometrical parameters influencing the sensitivity of a coplanar electrode layout for Electrical Impedance Flow Cytometry. The designs presented in this work have been simulated, fabricated and tested. 3D Finite Element Method was applied to simulate and improve the sensitivity of the coplanar designs for two spacings between electrodes. The proposed model uses conditional expressions to define spatially dependent material properties. The vertical and lateral sensitivities were evaluated for all the designs. The experimental results obtained with polystyrene beads show good agreement with the simulations. Precentering particles with dielectrophoresis allowed to control their position in the microchannel. The optimized designs are envisioned to be used for sizing and characterizing particles from single cells to cell aggregates.

1. Introduction

Electrical Impedance Flow Cytometry is a label-free technique for characterizing objects in suspension in a flowing liquid. The principle was described by Coulter in 1953 (Coulter 1953) and the devices became commonly known as Coulter counters. When a particle passes through a small aperture in a membrane connecting two reservoirs, the characteristics of the electrical path are modified and this modification is linked to the properties of the particle and the liquid. Originally used with direct current or low-frequency signals to assess the size, the principle was later extended by the use of multiple frequencies to enable the characterization of particle dielectric properties at higher frequencies (Coulter and Hogg 1970; Coulter and Rodriguez 1988).

In the late 90's, the principle was translated in microsystems in which thick electrodes of the size of a microchannel were patterned for fluid analysis (Ayliffe et al. 1999). Gawad et al (Gawad et al. 2001) alternatively

employed thin electrodes patterned in a microchannel for cell analysis and particle sizing and thereby pioneered the field of on-chip impedance flow cytometry. Since then, a broad variety of cell types have been investigated by impedance spectroscopy, including blood cells (erythrocytes (Cheung et al. 2005; Gawad et al. 2001; Kuttel et al. 2007), white blood cells (Han et al. 2012; Holmes and Morgan 2010; Holmes et al. 2009) and platelets (Evander et al. 2013)), cancer cells (Spencer et al. 2014; Zhao et al. 2016a; Zhao et al. 2014), microbes (yeast (Haandbaek et al. 2014a; Haandbaek et al. 2016; Shaker et al. 2014), bacteria (Haandbaek et al. 2014b), plankton (Benazzi et al. 2007)), stem cells (Song et al. 2016; Song et al. 2013; Zhao et al. 2016b), etc. More detailed information can be found in the reviews of Morgan et al. (Morgan and Spencer 2015; Sun and Morgan 2010), Chen et al. (Chen et al. 2015) and Petchakup et al. (Petchakup et al. 2017).

Two main electrode configurations have been proposed: the coplanar and the parallel microelectrodes, also called "facing electrodes". The coplanar design consists of two patterned electrodes located at the bottom of a microchannel. This design is sensitive to the height of the particle in the microchannel due to the electric field non-uniformity. Facing microelectrodes were proposed as an alternative by Gawad et al. (Cheung et al. 2005) and allowed to have a more homogeneous current density around the cell under measurement. In this configuration, the electrodes are located at the top and the bottom of the microchannel, creating a more homogeneous electric field distribution in a smaller volume, thus improving the sensitivity. However, this design requires a more complex fabrication process and the signal is still dependent on the cell position in the detection volume (Spencer and Morgan 2011).

The coplanar design has recently been reinvestigated because of its ease of fabrication. In order to improve this design, so-called "liquid electrodes" were utilized to reduce the effect of the field non-uniformity (Demierre et al. 2007). In this configuration, the electrodes are positioned at the bottom of dead-end chambers placed on each side of the main channel. This creates a homogeneous electric field over the channel height if the distance of the electrodes to the channel is at least equal to the channel height (Demierre 2008). However, the sensitivity is reduced due to a larger detection length and thus a larger detection volume.

More recently, a solution closer to a Coulter counter was proposed by Chen et al. (Chen et al. 2011) who used a constriction channel with a cross-sectional area smaller than the investigated cell. In this case, the impedance amplitude value obtained is increased due to the fact that the deformed cell occupies most of the detection volume. On the other hand, the risk of clogging is higher and only a small range of cell sizes can be used for each design.

In order to mitigate the positional dependence of the particle in the coplanar design, Caselli et al. (Caselli and Bisegna 2017; De Ninno et al. 2017) proposed to use multiple electrodes and to analyze the pulse shape to retrieve the position of the particle. The geometry was also reinvestigated by Clausen et al. (Clausen et al. 2014), who showed that tuning the design of the microchannel could improve the sensitivity of Electrical Impedance Flow Cytometry measurements. In their study, they demonstrated that doubling the electrode width allowed to increase the peak amplitude of more than 40 %. However, they only considered the effect of this parameter in their analysis.

Most of the work described in the literature focuses on analyzing a specific size of cell, hence most of the sensors are suited for only a certain range of particles. A design capable of sizing and characterizing single cells and small cell aggregates is still missing. We are interested in creating cell aggregates of controllable size in flow, which requires the capability to analyze both single cells and cell aggregates.

In this paper, we present a comprehensive study for the improvement of electrical impedance sensitivity of coplanar electrodes by investigating the influence of the microchannel design. The application is the characterization of single cells and small cell aggregates in a chip for dielectrophoresis-assisted creation of cell aggregates in flow conditions. The impedance sensor presented in this article is a building block of the final chip where cells can be counted by impedance as single particles before entering in a DEP-trapping chamber where they aggregate and, after release of the DEP voltage used for trapping, can be characterized as cell aggregates(Cottet et al. 2018 (Submitted)).

The general configuration is composed of a 50 μm square microchannel with a pair of 50 μm long coplanar electrodes at its bottom, separated by 50 or 150 μm. A detailed analysis of four designs is first performed through FEM (Finite Element Method) simulations with Comsol Multiphysics and the results are confronted with experimental measurements carried out on 8 μm diameter polystyrene beads. Frequently, in both facing and coplanar electrode layouts, a differential measurement is performed(Cheung et al. 2005; Clausen et al. 2014; Gawad et al. 2001). In this article, the goal is to study the influence of the design of the impedance sensor on the signal. To assess such influence, only an absolute measurement scheme is needed without the need of a differential measurement since the baseline subtraction can be done numerically.

2. Simulations

2.1. Simulated designs

A conventional Electrical Impedance Flow Cytometry chip with a straight channel design further named "conventional" design is used as a reference design and presented in Fig. 1 a). It consists of two coplanar electrodes at the bottom of the microchannel. A voltage is applied between the two electrodes and the current is recorded. The current drops when a particle flows between the electrodes. The proposed analysis method consists in studying the variation of the current drop while changing several parameters as defined in Fig. 1 b). The height, h, and width, w, of the microchannel are kept constant in the study (h = 50 µm and w = 50 µm) as well as the length of the electrodes, l_{el}, while the other parameters are varying.

The influence of the following parameters on the sensitivity is tested:

- The inter-electrode distance, d_{el}
- The width of the electrodes, w_{el}
- The length of the maximum sensitivity area, d
- The widening length, b
- The widening to electrode distance, a

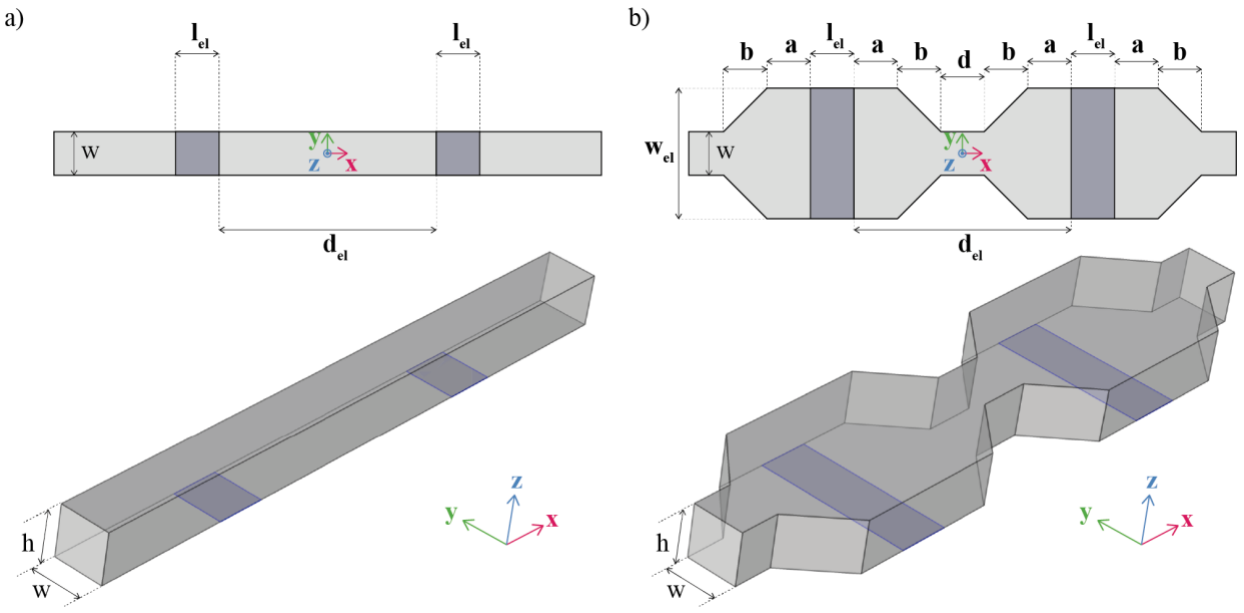

Fig. 1 Top view and 3D view of a) the conventional design and b) the conceptual design. l_{el} = 50 µm, h = 50 µm and w = 50 µm are kept constant. a, b, d, d_{el} and w_{el} are the parameters to optimize. Electrodes are represented in blue.

The dimensions used in this design were selected to allow the sizing of 8 µm diameter single cells as well as 50 µm diameter cell aggregates. Increasing the length of the electrodes, l_{el}, can theoretically increase the current between the electrodes but would lead to an increase of the capacitance between the electrodes. Furthermore, most current lines added by a longer electrode would be confined to the top of the microchannel. Therefore, l_{el} was fixed at 50 µm for the different designs to be equal to the height of the microchannel h.

2.2. Simulation specifications

The modeling of impedance variation was performed using Comsol Multiphysics 5.3 and the AC/DC Module. Comsol was used with Matlab R2016a via LiveLink to extend the modeling with scripting programming in the MATLAB environment. All the simulations performed aimed at studying the current variation due to an 8 µm diameter polystyrene bead positioned at the center of the detection volume (x = 0 µm, y = 0 µm, z = h/2 = 25 µm). The bead electrical conductivity and relative permittivity values were set to 5 x 10^{-6} S/m and 2.5, respectively. The conductivity and relative permittivity of the liquid between the electrodes were set to 1.6 S/m (Phosphate Buffer Saline conductivity) and 80, respectively.

The relative current variation was considered with respect to the current between the electrodes without a particle. A spherical particle was defined as a change in material properties instead of a geometrical entity. The particle was moved along the channel by displacing its center using a parametric sweep. More details on this method are available

in the supplementary material. An AC signal of amplitude 1.6 $V_{peak\text{-}to\text{-}peak}$ at 500 kHz was applied between the two electrodes. In the numerical model, the electrode capacitance is not taken into account as the frequency used for the impedance measurements is 500 kHz.

The meshing as well as the corresponding mesh convergence study are described in the supplementary material (Figure S1, S2 and S3), validating the choice of discretization.

2.3. Simulation results

2.3.1. Influence of d_{el}

The first parameter examined was the inter-electrode distance, d_{el}, in a conventional design, with $w = w_{el}$. The evolution of the current variation with d_{el} is presented in Fig. 2. As the distance between the electrodes increases from 40 to 180 μm, both the absolute and relative current variations decrease. Two different distances were chosen for further study: d_{el} = 50 μm, corresponding to the height of the microchannel and the diameter of the targeted aggregate, and d_{el} = 150 μm corresponding to three times the height of the microchannel. For d_{el} = 50 μm, the electric field is not homogeneous along the z axis, leading to a strong height dependence of the current variation but the sensitivity to passing particles is significant at any height. For d_{el} = 150 μm, the electric field is homogeneous along the z axis in the central cube (50 μm x 50 μm x 50 μm) offering a theoretically height-independent detection for both single particles and the entire aggregate. However, the overall sensitivity to single particles is reduced because of the smaller volume occupied by the particles compared to the inter-electrode volume. The designs with d_{el} = 50 μm and d_{el} = 150 μm will be referred to as “Short” and as “Long” respectively. The order of magnitude of the current variation induced by the passage of a bead, 0.1%, is in the same order of magnitude as the value reported by Spencer (Spencer and Morgan 2011).

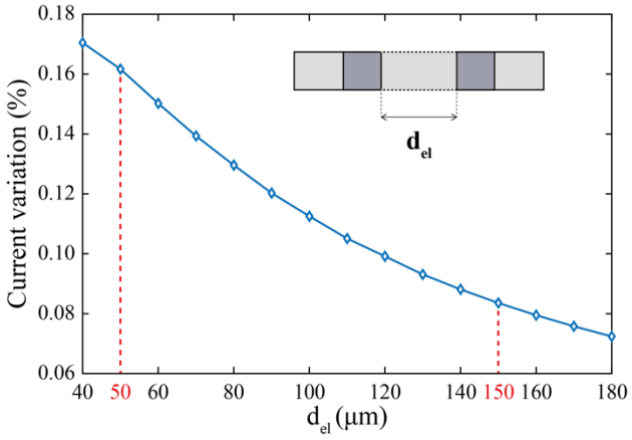

Fig. 2 Simulation of the evolution of the current variation with the inter-electrode distance d_{el} due to an 8 µm diameter polystyrene bead located at x = 0 µm, y = 0 µm and z = h/2 = 25 µm for w = w_{el} = 50 µm.

2.3.2. Influence of w_{el}

Increasing the width of the electrodes w_{el} will lead to a larger current flowing between the electrodes. For the two designs (Short and Long), the evolution of the current variation with w_{el} is displayed in Fig. 3 a) and b). In both cases the current variation increases with w_{el} until it reaches a final value. From the fluidic aspect w_{el} cannot be increased too drastically as it would lead to vorticity in the dead volumes. In both cases the increase was interpolated with an increasing exponential decay as displayed in Fig. 3 a) and b). w_{el} was chosen as the time when approximately 95% of the final value was reached, as a compromise between the maximum sensitivity and fluidic considerations. This corresponds to w_{el} = 90 µm and w_{el} = 140 µm for d_{el} = 50 µm and 150 µm, respectively. Details on the fitting parameters are given in Table S1 in the supplementary material.

2.3.3. Influence of b

Increasing the widening length, b, should reduce the current variation as the confinement of the electric field lines will be reduced due to a smoother transition between the electrode side and the maximum sensitivity area, d. At the same time, a small b value will correspond to a geometry presenting corners. Fig. 3 c) and d) shows the results for respectively a “Short” and a “Long” design.

In Fig. 3 c), a is fixed to 5 µm for fabrication considerations, 5 µm being the minimum distance for which the electrodes will still be on each side of the constriction. b is optimized and d is deduced from the geometric relation d + 2 * (a +b) = d_{el}. The decrease was interpolated with a polynomial decay and b was taken as 99% of the maximum value of b, as a compromise between the maximum sensitivity and fluidic considerations. It corresponds to b = 7 µm

and d = 26 µm. This design will be referred to as "Short Optimized" (SO) design and the original design with d_{el} = 50 µm as "Short Conventional" (SC) design. Details on the fitting parameters are given in Table S1 in the supplementary material.

In Fig. 3 d), d is fixed to 50 µm, to have the full central sensitive volume of the size of the aggregate, b is optimized and a is deduced from the geometric relation d + 2*(a + b) = d_{el}. Following the same methodology, we obtained b = 15 µm and a = 35 µm. This design will be referred to as "Long Optimized" (LO) design and the original design with d_{el} = 150 µm as "Long Conventional" (LC) design.

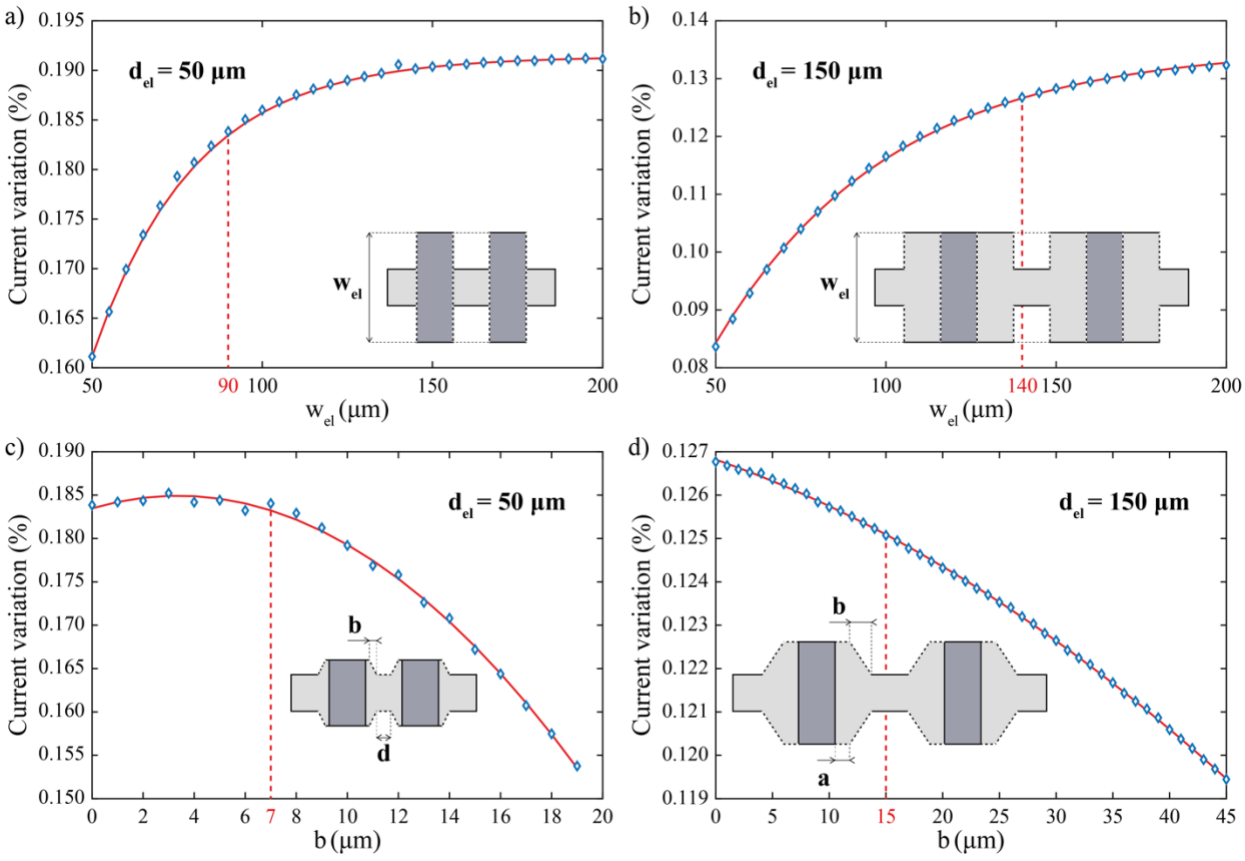

Fig. 3 Simulation of the current variation due to an 8 µm diameter polystyrene bead located at x = 0 µm, y = 0 µm, z = h/2 = 25 µm. Evolution with w_{el} for (a) d_{el} = d = 50 µm and (b) d_{el} = 150 µm with a = 50 µm, b = 0 µm, d = 50 µm. Evolution with b for (c) d_{el} = 50 µm for w_{el} = 90 µm, a = 5 µm, d = d_{el} – 2*(a + b) = 40 – 2b and (d) d_{el} = 150 µm for w = 50 µm, w_{el} = 140 µm, d = 50 µm, a = (d-d_{el})/2 - b = 50 – b. Fitted curves are displayed in red.

2.4. Proposed design for testing

All the geometrical parameters used for the four designs are summarized in Table 1. Fig. 4 presents the current variation due to an 8 µm diameter polystyrene bead located at y = 0 µm and z = h/2 = 25 µm for the four tested designs.

Design	h	l_{el}	w	d_{el} (*)	w_{el}	b	d	a
	µm	µm	µm	µm	µm	µm	µm	µm
SC	50	50	50	50	50	0	50	0
SO	50	50	50	50	**90**	**7**	**26**	5
LC	50	50	50	150	50	0	50	0
LO	50	50	50	150	**140**	**15**	50	**35**

Table 1 Geometrical parameters used for each design, optimized parameters are in bold, (*) indicates that the value was chosen but not optimized.

In an optimized design, the peak amplitude for a centered particle is increased with both inter-electrode distances: +14.4% for the Short design and +50.1% for the Long design compared to the corresponding conventional designs. In both cases, the peaks are sharper for the optimized designs.

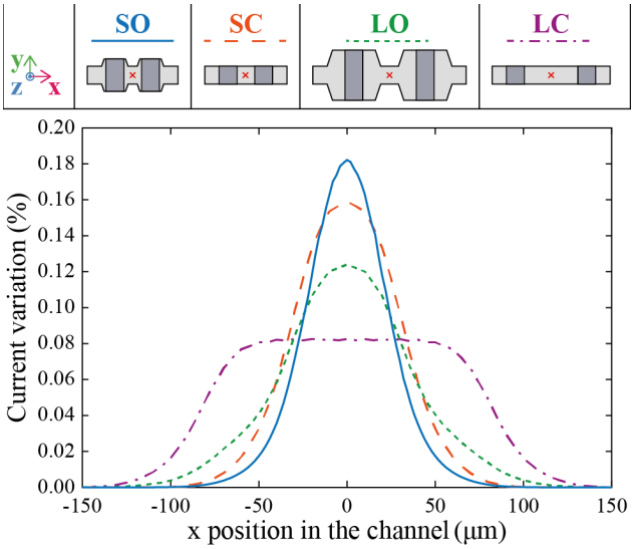

Fig. 4 Simulation of the current variation due to an 8 µm diameter polystyrene bead located at (y = 0 µm, z = h/2 = 25 µm). Evolution with the x position in the microchannel for the 4 designs: Short Optimized (SO), Short Conventional (SC), Long Optimized (LO) and Long Conventional (LC). The red cross indicates the point (x=0, y=0) on each design.

Fig. 5 shows the evolution of the current variation for each design for an 8 µm diameter polystyrene bead with (a) the y position of the particle located at x = 0 µm and z = h/2 = 25 µm and with (b) the z position of the particle located at x = 0 µm and y = 0 µm. In the case of the Short designs, the current variation is very dependent on both the lateral and vertical positions of the particle.

Concerning the lateral position, for the SO design, the variation of the current variation will be 32% greater near the wall in respect to the variation linked to a centered particle. For the SC design, it will be of 3.2%. For the Long design, those variations will be of 10.9% and 3.2% for the L0 and LC designs respectively. Optimized designs are more sensitive to the y position hence requiring some lateral focusing.

Concerning the z position, the Short designs are more sensitive to the vertical position of the particle than the Long designs. The most sensitive design is the SC design with +70.5%/-26.9% of variation of the current variation compared to a z-centered particle (z = h/2 = 25 µm), considering the lowest/highest z positions of the particle (z = 5 µm and z = 45 µm). The SO design is a bit less sensitive with +48.7%/-18.5%. The Long designs are less sensitive to the z position of the particle with +4%/-2.3% and +5.1%/-1.3% for the LO and LC designs respectively.

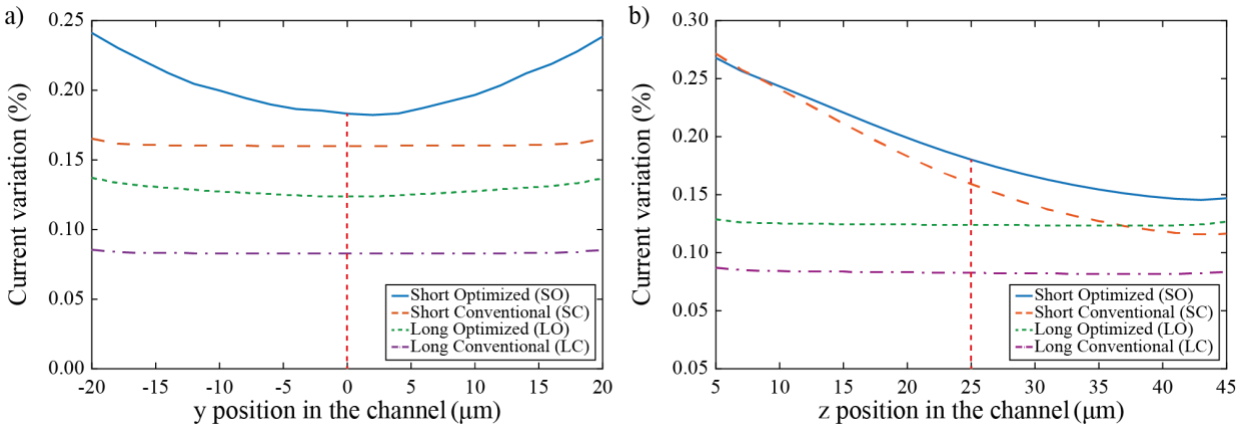

Fig. 5 Simulation of the current variation due to an 8 µm diameter polystyrene bead for the 4 designs. Evolution with (a) the y position in the microchannel (located at x = 0 µm, z = h/2 = 25 µm) and with (b) the z position in the microchannel (located at x = 0 µm, y = 0 µm). The red vertical dotted line represents the position of the particle in the center (x = 0 µm, y = 0 µm and z = 25 µm).

2.5. Vertical and longitudinal position sensitivity

For each design, the evolution of the current variation with the x position in the channel at different heights is displayed in Fig. 6. The Short designs are very sensitive to the height of the particle, as can be noticed both in the shape and in the amplitude compared to the Long designs.

The Long designs are sensitive to the height of the particle mostly in the shape but the amplitude of the current variation in the central zone (x = 0 µm) varies little and hence will be mostly linked to the size of the particle.

For the conventional designs (SC and LC), when the particle passes close to the electrodes (mostly z = 5 µm), the shape of the peak is not just a drop but is strongly M-shaped. This is due to the fact that when the particle passes near the electrode (low heights) in the conventional design, the perturbation is higher than when the particle is in the middle of the detection area (x = 0 µm). This particular peak form is also observed in the case of Coulter counters when the particle passes close to the wall of the aperture (Allen 1997). For the SO design, the M shape is only present when the particle passes very close to the electrodes. In the case of the LO design, the M-shaped curve is also present but the

maxima are only local maxima and the global maximum is in the central part of the channel (x = 0 µm). In the optimized designs, as the electrode is wider, the passing of a particle close to the electrode induces less variation than in the conventional designs.

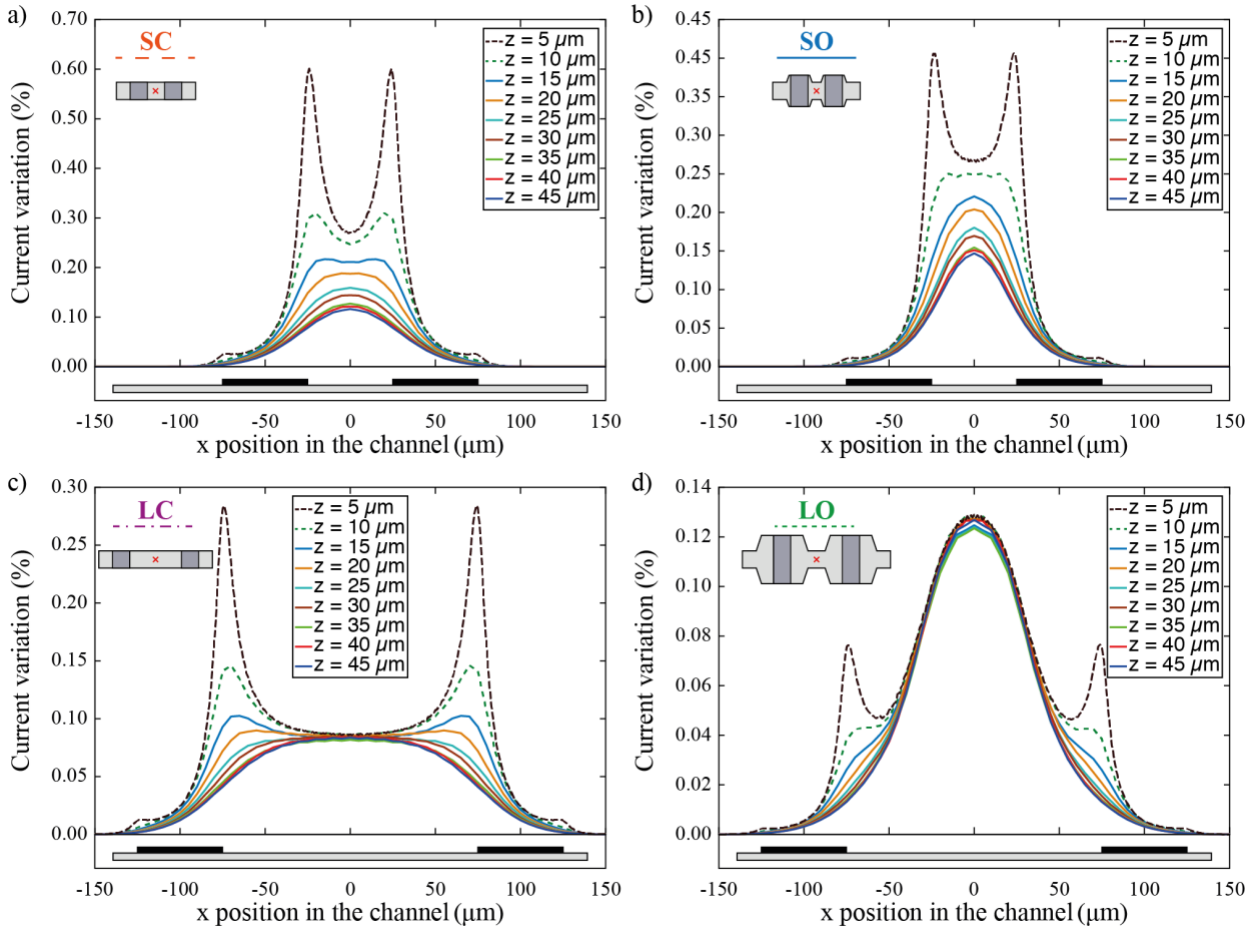

Fig. 6 Simulation of the current variation due to an 8 µm diameter polystyrene bead. Evolution with the x position in the microchannel (located at y = 0 µm) at different heights for the 4 designs: (a) SC (b) SO (c) LC (d) LO. Electrode positions (in black) are indicated under each graph.

3. Laboratory experiments

3.1. Fabrication

The four designs were fabricated on two chips: each chip contains in the middle 9 electrodes used for DEP centering, and on both sides a combination of the 3 designs, symmetrically (SC, LC and either SO or LO).

The electrodes were fabricated through a standard photolithography process. 200 nm of platinum were sputtered on a 4-inch float glass wafer with 20 nm titanium adhesion layer. A positive photoresist (AZ1512 - 1.5 µm) was then coated using an ACS 200 automatic wafer coater and developer (SUSS MicroTec – Garching, Germany), and

structured through direct writing with a WaferWriter MLA150 (Heidelberg Instrument – Heidelberg, Germany) before being developed with the ACS 200. The Ti/Pt layer was later etched with Ion Beam Etching (IBE) up to the glass layer. Finally, the photoresist was stripped and the glass substrate with Ti/Pt electrodes was obtained. Afterwards, the wafer was diced to separate all the chips.

The microfluidic layer was created using a silicon mold for PDMS. The mold was fabricated starting with a Silicon-On-Insulator (SOI) wafer (handle wafer Si (thickness 380 µm) – buried oxide (thickness 2 µm)– device wafer Si (thickness 50 µm)). The wafer was coated with a positive photoresist (AZ1512 - 2 µm) with the ACS 200, patterned with the MLA 150 (with a design scaled by a factor of 1.015 to compensate the PDMS shrinkage) and then developed with the ACS 200. The patterned silicon layer was etched with the Bosch process until the buried oxide layer was reached (with an Adixen AMS200 Deep Reactive Ion Etching etcher from Alcatel Micro Machining Systems, Annecy – France). The photoresist was later stripped from the wafer which was next silanized with Trichloro (1H,1H,2H,2H-perfluorooctyl)silane (PFOTS from Sigma Aldrich). PDMS was subsequently poured on the wafer, cured at 80°C for 2h before demolding, separating the PDMS slabs and punching the access holes. The PDMS slabs were aligned afterward with the electrodes using a mask aligner. For more details on fabrication, see Cottet et al. (2017)(Cottet et al. 2017).

The different fabricated designs are presented in Fig. 7.

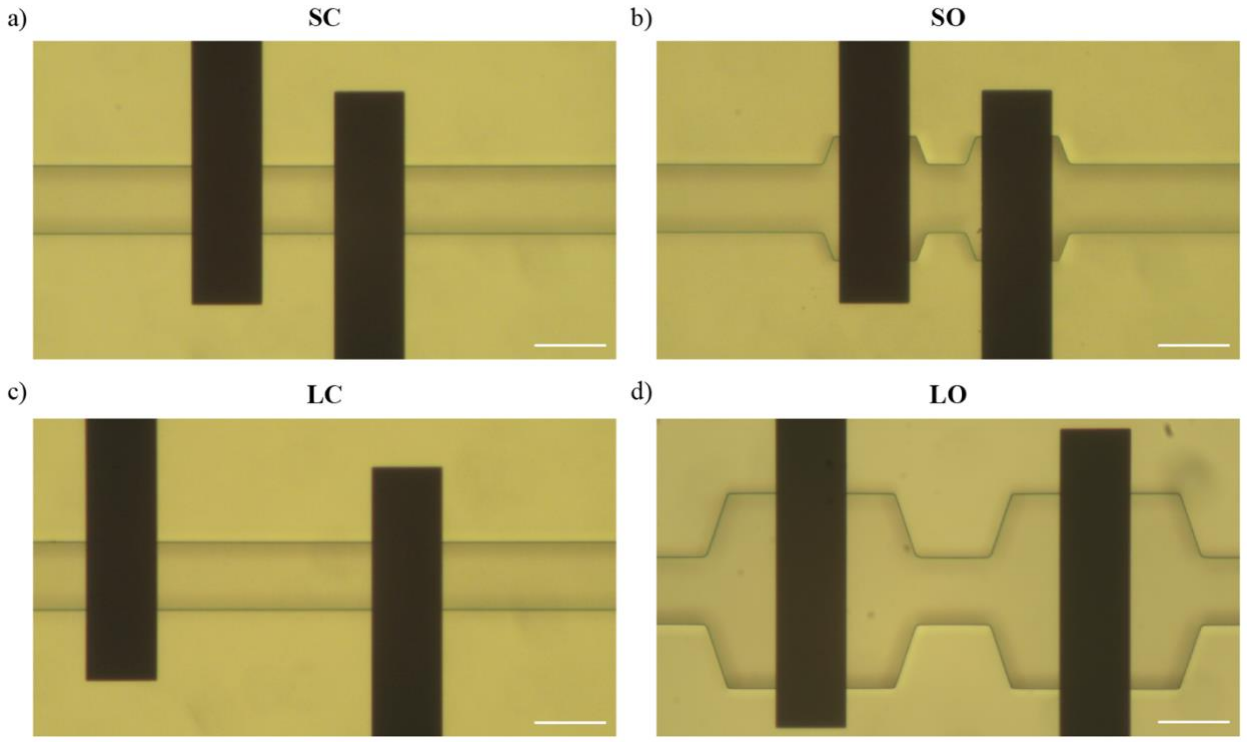

Fig. 7 Photographs of the different designs (a) SC (b) SO (c) LC (d) LO. Scalebar 50 µm. Ti/Pt Electrodes are visible as black stripes.

3.2. Experimental setup

Fig. 8 presents the schematic representation of the experimental setup used. 20 $V_{peak\text{-}to\text{-}peak}$ at 100 kHz were applied on the dielectrophoresis (DEP) focusing electrodes to center the particles laterally(Braschler et al. 2008; Demierre et al. 2008) and to provide a vertical lifting(Shaker et al. 2014).

Impedance measurements were performed by applying an AC signal of 1.6 $V_{peak\text{-}to\text{-}peak}$ amplitude at a frequency of 500 kHz on one electrode and amplifying the current change on the other electrode using an HF2TA current amplifier (Zurich Instruments, Zurich – Switzerland). The current was demodulated with an HF2LI Lock-In amplifier (Zurich Instruments, Zurich – Switzerland).

The channel was filled first with PBS (1.6 S/m) prior to the experiment using a Nemesis syringe pump. A suspension of 8 µm diameter polystyrene beads (Sigma Aldrich, Buchs – Switzerland) in PBS at 3.5 x 10^5 beads/mL was prepared and then perfused at 10 µL/h during the experiment to provide a flow rate similar to the one that would be used for DEP trapping of cells in flow(Cottet et al. 2018 (Submitted)). Therefore, the DEP centering module enables

to have a reproducible height of the particles at low flow rates. Experimental data were recorded and further processed with Matlab.

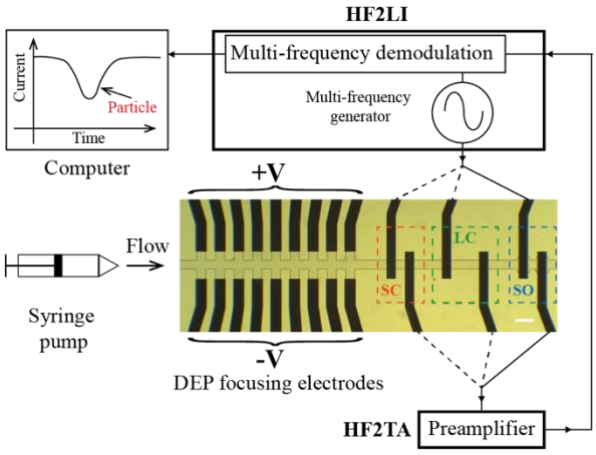

Fig. 8 Schematic representation of the system with a photograph of the chip showing 3 designs. Scalebar 100 µm.

4. Results and discussion

Fig. 9 presents the experimental results obtained for the four different designs. In the SO and LO designs, the velocity of a particle passing through is not constant due to the widening of the microchannel. For this reason, the time scale in Fig. 9 was not converted into a distance scale. The laboratory experiments are in good agreement with the simulations. The relative amplitudes of the curves at t = 0 ms (particle at x = 0) are similar to what was predicted by the simulations (cf Fig. 4 and Fig. 6). According to observations with the microscope and to the standard dispersion observed in Fig. 9. the shape of each curve corresponds to a particle centered laterally with DEP. The M-shape curves observed for the conventional designs (SC and LC) indicate that the particle is not centered vertically. According to the amplitude of the peak and the M-shape we can estimate the height of the center of the particles between 5 and 15 µm. At this flow rate (10 µL/h) the DEP forces overcome sedimentation but are insufficient to lift the particles up to the center of the channel.

Details on the data processing can be found in the supplementary material with Figure S4.

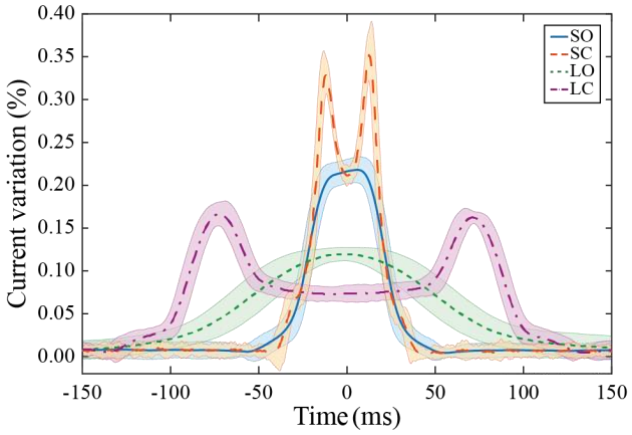

Fig. 9 Experimental data showing the evolution with time of the average current variation for each design with +/- 2 times the standard deviation (n>=8) due to an 8 µm diameter polystyrene bead in the microchannel for the 4 designs. Measurements were peformed for the 4 designs at a flow rate of 10 µL/h (particle speed in the order of 1000 µm/s).

Both simulations and laboratory experiments provided insights on the performances of each design. The "Short" designs provide a higher signal when a particle is passing between the electrodes compared to the "Long" ones. The Short Conventional design (SC) provides a signal highly dependent both in shape and in amplitude on the height of the particle in the microchannel. The M shape obtained could be analyzed to determine the height of the particles. One of the challenges is to have enough points on the experimental curve to determine precisely the amplitude of the M. The signal could, however, be misinterpreted as two particles closely following each other. The model presented in this manuscript is intended to be used with a small cell concentration. However, in case of doublets, the current variation is relatively higher than for a single particle passing. Furthermore, the shape of the peak is modified. In case of separated particles passing through the detection area at the same time, a similar conclusion is still valid: higher variation of the current variation and/or two peaks close to each other depending of the distance between the particles.

The Short Optimized design (SO) provides a signal amplitude which is still dependent on the particle height but the experimentally observed shape is a single peak. The peak shape height dependency is less pronounced for this design: the M shape only occurs on very low heights and is not observed experimentally thanks to the DEP lifting. The Long designs provide a broader signal because of a longer transition time between the electrodes. In the Long Conventional design (LC), the current variation at the center does not depend on the particle height. However, off-center, the current variation is higher and the related peak amplitude is height dependent. Finally, for the Long Optimized design (LO), there is only a single peak whose amplitude does not depend on the particle height. The current density at x = 0 µm for each design is displayed in Figure S5 of the supplementary material.

The sensitivities to the longitudinal fabrication misalignment (along the x axis) of the optimized designs are presented in Figure S6 of the supplementary material. For a misalignment of 5 μm, this would result in a variation of the current variation of 0.5% for SO and 0.02% for LO compared to the respective references without longitudinal misalignment. Analysis of fabrication results presented in Cottet et al. (2017) (Cottet et al. 2017) showed that the maximum misalignment obtained was in all cases less than 5 μm as can also be seen in Fig. 7.

The best candidate for our application, characterization of particles at very low flow rate with a relatively insensitivity to the particle height, is the Long Optimized design. Peak detection algorithms, after adjustment, will find central peaks in all cases (Brazey et al. 2018). This design is also insensitive to longitudinal misalignment in the fabrication process. As 8 μm polystyrene beads were used to perform all the optimization simulations, it was considered as the lower limit for the particle diameter. Different diameters were simulated for the Long Optimized (LO) design and the results show that the current variation significantly increases when the particle diameter increases but does not depend on the electrical conductivities of the medium as illustrated in Table 2. The value of the electrical conductivity should be chosen according to the application: a high conductivity to obtain more signal for impedance sensing only and a lower conductivity if the sensor should be integrated in a chip with for example DEP trapping to reduce Joule heating.

Particle diameter	Current variation (in %)	
(in µm)	σ_m = 1.6 S/m	σ_m = 0.16 S/m
8	0.1193	0.1193
10	0.2507	0.2495
12	0.4194	0.4178
14	0.6749	0.6732
16	1.0006	0.9995
18	1.4375	1.4341
20	1.9725	1.9638
22	2.6571	2.6494
24	3.4516	3.4434
26	4.4685	4.4558
28	5.5781	5.5657
30	6.9738	6.9619
32	8.5453	8.5241
34	10.4399	10.4135
36	12.5886	12.5617
38	15.1498	15.1200
40	18.0046	17.9733
42	21.5098	21.4709
44	25.4324	25.3903
46	30.3095	30.2645
48	36.0182	35.9647

Table 2 Comparison of the simulated influence of the different diameters of polystyrene beads (located at x = 0 µm, y = 0 µm and z = h/2 = 25 µm) on the current variation for a Long Optimized (LO) design for two different electrical conductivities of the medium (σ_m = 1.6 S/m and σ_m = 0.16 S/m).

The evolution of the current variation for a 30 µm diameter particle in the LO design is displayed in Figure S7 of the supplementary material.

5. Conclusions

In this paper, we describe a comprehensive methodology for improving the sensitivity of a coplanar electrode design by modifying the microchannel geometry. The results of the simulations were tested experimentally. The methodology described in this work can be applied for any size of channels. More importantly, two optimized designs were proposed and validated: depending on the specifications of the application (centering method, flow speed, acquisition setup, etc) one of the optimized design would be preferred to the other. In particular, the Short Optimized design (SO) provides a maximum signal for centered particles (in all directions) and the Long Optimized (LO) is relatively insensitive to the particle height while giving more signal than the conventional one. This conclusion would be applicable in general.

For our application, the Signal-to-Noise ratio (SNR) should be sufficient to detect single cells in a relatively large channel. For all designs the SNR was sufficient to enable good detection of 8 μm diameter particles (Fig S4 of the supplementary material displays the signal obtained with the SO design).

The designs could be tested at higher flow rates to better overcome sedimentation. This should result in a smaller standard variation and better assessment of the size of the particle for all designs. However, the transition time of the particle between the electrodes will be shorter hence reducing the number of points measured. The variation of the current with the particle size could be validated experimentally.

Combining our optimized geometries (SO and LO) with more electrodes, as recently proposed by De Ninno et al.(De Ninno et al. 2017). would enable a better characterization of the particles moving between the electrodes, even for the lateral position(Reale et al. 2018). The designs are envisioned to be used for sizing and characterizing particles from single cells to cell aggregates. In the future, different sizes of particles will be used, as well as different cell types.

Conflicts of interest

There are no conflicts to declare.

Acknowledgements

The authors acknowledge the support from the CMi staff at EPFL for their technical assistance. The Ampere lab would like to acknowledge support from the Institut National de la Santé et de la Recherche Médicale (INSERM, Plan Cancer, Physicancer Program, Dynamo project). The authors also acknowledge the support of the Programme d'Avenir Lyon Saint-Etienne (PALSE mobility grant) and the Laboratoire d'Excellence iMUST (ANR-10-LABX-0064/ANR-11-IDEX-0007) from University of Lyon as well as the Doctoral school 160 EEA of the University of Lyon for the mobility grants allocated.

REFERENCES

Allen T (1997) Volume 1: Powder sampling and particle size measurement. In: Particle Size Measurement. Springer Netherlands, p 335

Ayliffe HE, Frazier AB, Rabbitt RD (1999) Electric impedance spectroscopy using microchannels with integrated metal electrodes Journal of Microelectromechanical Systems 8:50-57 doi:10.1109/84.749402

Benazzi G, Holmes D, Sun T, Mowlem MC, Morgan H (2007) Discrimination and analysis of phytoplankton using a microfluidic cytometer Iet Nanobiotechnology 1:94-101 doi:10.1049/iet-nbt:20070020
Braschler T, Demierre N, Nascimento E, Silva T, Oliva AG, Renaud P (2008) Continuous separation of cells by balanced dielectrophoretic forces at multiple frequencies Lab Chip 8:280-286 doi:10.1039/b710303d
Brazey B, Cottet J, Bolopion A, Van Lintel H, Renaud P, Gauthier M (2018) Impedance-based real-time position sensor for lab-on-a-chip devices Lab Chip 18:818-831 doi:10.1039/c7lc01344b
Caselli F, Bisegna P (2017) Simulation and performance analysis of a novel high-accuracy sheathless microfluidic impedance cytometer with coplanar electrode layout Med Eng Phys 48:81-89 doi:10.1016/j.medengphy.2017.04.005
Chen J, Xue C, Zhao Y, Chen D, Wu MH, Wang J (2015) Microfluidic impedance flow cytometry enabling high-throughput single-cell electrical property characterization Int J Mol Sci 16:9804-9830 doi:10.3390/ijms16059804
Chen J et al. (2011) Classification of cell types using a microfluidic device for mechanical and electrical measurement on single cells Lab Chip 11:3174-3181 doi:10.1039/c1lc20473d
Cheung K, Gawad S, Renaud P (2005) Impedance spectroscopy flow cytometry: on-chip label-free cell differentiation Cytometry Part A 65:124-132 doi:10.1002/cyto.a.20141
Clausen C, Skands G, Bertelsen C, Svendsen W (2014) Coplanar Electrode Layout Optimized for Increased Sensitivity for Electrical Impedance Spectroscopy Micromachines 6:110-120 doi:10.3390/mi6010110
Cottet J, Kehren A, Lasli S, van Lintel H, Buret F, Frénéa-Robin M, Renaud P (2018 (Submitted)) Dielectrophoresis-assisted creation of cell aggregates under flow conditions using planar electrodes
Cottet J, Vaillier C, Buret F, Frenea-Robin M, Renaud P (2017) A reproducible method for mum precision alignment of PDMS microchannels with on-chip electrodes using a mask aligner Biomicrofluidics 11:064111 doi:10.1063/1.5001145
Coulter WH (1953) Means for counting particles suspended in a fluid. US Patent,
Coulter WH, Hogg WR (1970) Signal modulated apparatus for generating and detecting resistive and reactive changes in a modulated current path for particle classification and analysis.
Coulter WH, Rodriguez CM (1988) Particle analyzer for measuring the resistance and reactance of a particle.
De Ninno A, Errico V, Bertani FR, Businaro L, Bisegna P, Caselli F (2017) Coplanar electrode microfluidic chip enabling accurate sheathless impedance cytometry Lab Chip 17:1158-1166 doi:10.1039/C6LC01516F
Demierre N (2008) Continuous-flow separation of cells in a lab-on-a-chip using "liquid electrodes" and multiple-frequency dielectrophoresis. EPFL doi:10.5075/epfl-thesis-4099
Demierre N, Braschler T, Linderholm P, Seger U, van Lintel H, Renaud P (2007) Characterization and optimization of liquid electrodes for lateral dielectrophoresis Lab Chip 7:355-365 doi:10.1039/b612866a
Demierre N, Braschler T, Muller R, Renaud P (2008) Focusing and continuous separation of cells in a microfluidic device using lateral dielectrophoresis Sensors and Actuators B-Chemical 132:388-396 doi:10.1016/j.snb.2007.09.078
Evander M, Ricco AJ, Morser J, Kovacs GTA, Leung LLK, Giovangrandi L (2013) Microfluidic impedance cytometer for platelet analysis Lab Chip 13:722-729 doi:10.1039/c2lc40896a

Gawad S, Schild L, Renaud PH (2001) Micromachined impedance spectroscopy flow cytometer for cell analysis and particle sizing Lab Chip 1:76-82 doi:10.1039/b103933b
Haandbaek N, Burgel SC, Heer F, Hierlemann A (2014a) Characterization of subcellular morphology of single yeast cells using high frequency microfluidic impedance cytometer Lab Chip 14:369-377 doi:10.1039/c3lc50866h
Haandbaek N, Burgel SC, Rudolf F, Heer F, Hierlemann A (2016) Characterization of Single Yeast Cell Phenotypes Using Microfluidic Impedance Cytometry and Optical Imaging Acs Sensors 1:1020-1027 doi:10.1021/acssensors.6b00286
Haandbaek N, With O, Burgel SC, Heer F, Hierlemann A (2014b) Resonance-enhanced microfluidic impedance cytometer for detection of single bacteria Lab Chip 14:3313-3324 doi:10.1039/c4lc00576g
Han XJ, van Berkel C, Gwyer J, Capretto L, Morgan H (2012) Microfluidic Lysis of Human Blood for Leukocyte Analysis Using Single Cell Impedance Cytometry Anal Chem 84:1070-1075 doi:10.1021/ac202700x
Holmes D, Morgan H (2010) Single Cell Impedance Cytometry for Identification and Counting of CD4 T-Cells in Human Blood Using Impedance Labels Anal Chem 82:1455-1461 doi:10.1021/ac902568p
Holmes D et al. (2009) Leukocyte analysis and differentiation using high speed microfluidic single cell impedance cytometry Lab Chip 9:2881-2889 doi:10.1039/b910053a
Kuttel C, Nascimento E, Demierre N, Silva T, Braschler T, Renaud P, Oliva AG (2007) Label-free detection of Babesia bovis infected red blood cells using impedance spectroscopy on a microfabricated flow cytometer Acta Trop 102:63-68 doi:10.1016/j.actatropica.2007.03.002
Morgan H, Spencer D (2015) Microfluidic Impedance Cytometry for Blood Cell Analysis. In: Microfluidics for Medical Applications. The Royal Society of Chemistry, pp 213-241. doi:10.1039/9781849737593-00213
Petchakup C, Li KHH, Hou HW (2017) Advances in Single Cell Impedance Cytometry for Biomedical Applications Micromachines 8 doi:10.3390/mi8030087
Reale R, De Ninno A, Businaro L, Bisegna P, Caselli F (2018) Electrical measurement of cross-sectional position of particles flowing through a microchannel Microfluid Nanofluid 22 doi:10.1007/s10404-018-2055-3
Shaker M, Colella L, Caselli F, Bisegna P, Renaud P (2014) An impedance-based flow microcytometer for single cell morphology discrimination Lab Chip 14:2548-2555 doi:10.1039/c4lc00221k
Song HJ et al. (2016) Identification of mesenchymal stem cell differentiation state using dual-micropore microfluidic impedance flow cytometry Anal Methods-Uk 8:7437-7444 doi:10.1039/c6ay01377e
Song HJ, Wang Y, Rosano JM, Prabhakarpandian B, Garson C, Pant K, Lai E (2013) A microfluidic impedance flow cytometer for identification of differentiation state of stem cells Lab Chip 13:2300-2310 doi:10.1039/c3lc41321g
Spencer D, Hollis V, Morgan H (2014) Microfluidic impedance cytometry of tumour cells in blood Biomicrofluidics 8 doi:10.1063/1.4904405
Spencer D, Morgan H (2011) Positional dependence of particles in microfludic impedance cytometry Lab Chip 11:1234-1239 doi:10.1039/c1lc20016j
Sun T, Morgan H (2010) Single-cell microfluidic impedance cytometry: a review Microfluid Nanofluid 8:423-443 doi:10.1007/s10404-010-0580-9

Zhao Y et al. (2016a) Single-Cell Electrical Phenotyping Enabling the Classification of Mouse Tumor Samples Sci Rep 6:19487 doi:10.1038/srep19487
Zhao Y et al. (2016b) Electrical property characterization of neural stem cells in differentiation PLoS ONE 11 doi:10.1371/journal.pone.0158044
Zhao Y et al. (2014) Tumor cell characterization and classification based on cellular specific membrane capacitance and cytoplasm conductivity Biosensors Bioelectron 57:245-253 doi:10.1016/j.bios.2014.02.026